Advances in Radiation Oncology (2016) **1**, 365-372

advances
in radiation oncology

www.advancesradonc.org

Scientific Article

Functional imaging equivalence and proof of concept for image-guided adaptive radiotherapy with fixed gantry and rotating couch

Ilana Feain PhD [a,*], Chun-Chien Shieh PhD [a], Paul White MMedPhys [b], Ricky O'Brien PhD [a], Sandra Fisher MMedPhys [b], William Counter PhD [a], Peter Lazarakis PhD [a], David Stewart BRadTherapy [b], Simon Downes MMedPhys [b], Michael Jackson MBBS [c], Siddhartha Baxi MBBS [d], Brendan Whelan PhD [a,e], Kuldeep Makhija BSc [a], Chen-Yu Huang PhD [a], Michael Barton MBBS [e], Paul Keall PhD [a]

[a] *Radiation Physics Laboratory, Central Clinical School, The University of Sydney, Sydney, New South Wales, Australia*
[b] *Department of Radiation Oncology, Nelune Comprehensive Cancer Centre, Prince of Wales Hospital, Randwick, New South Wales, Australia*
[c] *Department of Radiation Oncology, School of Medicine, University of New South Wales, Randwick, New South Wales, Australia*
[d] *Department of Radiation Oncology, South West Radiation Oncology Service, Bunbury, Western Australia, Australia*
[e] *Collaboration for Cancer Outcomes Research and Evaluation (CCORE), Ingham Institute for Applied Medical Research, University of New South Wales, Liverpool, New South Wales, Australia*

Received 31 December 2015; received in revised form 12 October 2016; accepted 19 October 2016

Abstract

Purpose: The purpose of this article is to present the first imaging experiments to demonstrate the functional equivalence between a conventional rotational gantry and a fixed-beam imaging geometry, and the feasibility of an iterative image-reconstruction technique under gravitational deformation.

Methods and materials: Experiments were performed using an Elekta Axesse with Agility MLC and XVI, a custom-built rotating phantom stage, a Catphan QA phantom, and a porcine heart. For

Sources of support: The authors gratefully acknowledge support from a National Health and Medical Research Council (NHMRC) Australia Fellowship and an Australian Research Council Linkage Infrastructure, Equipment and Facilities (ARC LIEF) grant.

Conflicts of interest: Feain, Shieh, and Keall are inventors on several pending patents related to Nano-X technology and image processing. Feain and Keall are directors of Nano-X Pty, Ltd.

* Corresponding author. Central Clinical School, The University of Sydney, Level 4, Blackburn Building D06, Camperdown Campus, Sydney 2006, Australia.

E-mail address: ilana.feain@sydney.edu.au (I. Feain)

http://dx.doi.org/10.1016/j.adro.2016.10.004

the imaging equivalence, a conventional cone beam computed tomography (CBCT) of the Catphan was acquired, as well as a set of 660 x-ray projections with a static gantry and rotating Catphan. Both datasets were reconstructed with the Feldkamp-Davis-Kress (FDK) algorithm, and the resultant volumetric images were compared using standard metrics. For imaging under gravitational deformation, a conventional CBCT of the Catphan and a set of 660 x-ray projections with a static gantry and rotating Catphan were also acquired with a porcine heart. The conventional CBCT was reconstructed using FDK. The projections that were acquired with the heart rotating were sorted into angular bins and reconstructed with prior image constrained compressed sensing using a deformation-blurred FDK prior. Deformation was quantified with B-spline transformation-based deformable image registration.

Results: For imaging equivalence, the difference between the two Catphan images was consistent with Poisson noise. For imaging under gravitational deformation, the conventional CBCT porcine heart image (ground truth at 0 degrees) matched the static gantry, rotating heart reconstruction with a mean magnitude of <3 mm and maximum magnitude of <5 mm of the deformation vector field. The mean deformation of the rotating heart was 3.0 to 8.9 mm, up to 16.1 mm maximum deformation. Deformation was mainly observed in the direction of gravity.

Conclusions: We have demonstrated imaging equivalence in cone beam CT reconstructions between rigid phantom images acquired with a conventional rotating gantry and with a fixed-gantry and rotating phantom. We have presented a method for image reconstruction under a fixed-beam imaging geometry using a deformable phantom.

Introduction

Cancer is the greatest economic health burden in the world, costing the global economy more than 2 trillion U.S. dollars annually.[1] It is a leading cause of noncommunicable disease and accounts for 1 of every 5 deaths worldwide. In 2012, 14.1 million cases of cancer were diagnosed and 8.2 million deaths were recorded. These numbers are expected to almost double by 2035.[2] Globally, radiotherapy is the recommended treatment for 50% to 60% of all patients with cancer.[3,4] It is estimated that there are currently 13,462 radiotherapy machines globally.[5] By 2035, the world will need an additional 21,800 machines just to meet increased treatment demands.[6]

The availability of radiotherapy machines is proportional to the gross national income per capita.[6,7] Major barriers to the provision of radiotherapy services in low- and middle-income countries include high capital and startup costs, high operational and servicing costs, provision of adequately trained staff, inadequacy of complex machines in areas that lack supportive infrastructure, and the large geographic distances that patients are required to travel to seek treatment.[8] There are simply not enough facilities to treat the increasing cancer epidemic; and patients in the lowest socioeconomic demographics are those who miss out most often. Globally, 55 countries have no radiotherapy at all, and tens of others are severely underserved.[6]

Geographic disparities in cancer outcomes due to radiotherapy accessibility in upper-middle- and high-income countries are also well established.[8-12] Lack of appropriately tailored (or any) radiotherapy services affect healthcare systems through increased patient morbidity and mortality, longer and more complicated hospitalizations, expensive medicines,[13] and unnecessary surgeries such as mastectomy and prostatectomy.[10,14,15] In Australia, for example, mortality rates are 35% higher for patients with cancer in rural areas[10,16] compared with mortality rates for patients with rectal cancer, which rise by 6% for every extra 100 km patients live from a radiotherapy clinic.[17] Indigenous patients with cancer suffer mortality rates that are 30% higher.[18,19]

Time for a change in approach

There is little doubt that innovative solutions to deliver high-quality, safe, affordable, and appropriate care are urgently needed to redress the staggering global underutilization of radiotherapy to treat the world's growing cancer epidemic.[20] There is also little doubt that the crisis is worsening, mainly in middle-income countries and at rates that are far greater than those in high-income countries, due largely to their greater population growth and longevity.[2] There is an urgent need, supported recently by the increasing number of global awareness campaigns, for innovative and economic solutions to deliver affordable and accessible

radiotherapy to patients worldwide. Manufacturers are responding by launching compact and less costly versions of some machines in a number of countries and regions.[21-23] Despite these efforts, the "silent crisis" continues unabated.[7]

Fixed-beam image-guided adapted radiotherapy machine

With a view to increase global access to affordable radiotherapy, static gantry, rotating patient systems are being developed. Eslick and Keall[24] previously introduced the concept of a compact, economic, real-time, image-guided, linear accelerator for radiotherapy with a small industrial footprint and a much smaller and more economic bunker design (Fig 1). The machine is designed to treat patients with a fixed vertical treatment beam, a fixed kilovoltage (kV) imaging system, and a patient rotation couch. It employs real-time tumor visualization and beam tracking. This decreases both capital and operational costs by reducing the engineering complexity, industrial footprint, and shielding requirements of the bunker.[24]

The purpose of this paper is to present the first imaging experiments for static gantry, fixed-beam, and rotating phantom imaging. The purpose of these experiments is to demonstrate the functional imaging equivalence between conventional rotational and fixed-beam imaging geometries and the feasibility of an image-reconstruction technique under rotation and gravitational deformation.

Methods and materials

Imaging equivalence under a fixed-beam, horizontal rotation geometry

A Catphan-computed tomography imaging QA phantom (Phantom Laboratory Inc., Greenwich, NY) was mounted onto the Phantom Rotation Platform. The phantom center or platform rotational axes were then aligned to isocenter. A conventional cone beam computed tomography (CBCT) was acquired with the LINAC kilovoltage imaging system, XVI in 'VolumeView' mode with the Phantom Rotation Platform static and orientated at an angle of 0 degrees. A second set of 660 x-ray projections was acquired with XVi (using the MotionView Scan Preset) while the gantry was static and the Phantom Rotation Platform rotated at 3 degrees/s. This speed was chosen to match the number of projections and the gantry velocity used under the CBCT acquisition. For the x-ray scans, the gantry was positioned for a vertical anterior megavolt (MV) beam so that the kV tube was set in a horizontal orientation with respect to the phantom. Both the conventional CBCT and x-ray projection images were reconstructed using back projection with the standard Feldkamp-Davis-Kress (FDK) algorithm.[25]

Image guidance under gravitational deformation

We repeated the method described with a porcine heart secured and mounted to the Phantom Rotation Platform. A separate CBCT was taken with the platform rotated to 0 degrees for comparison with the static gantry reconstruction method.

Our static gantry system had a fixed kV imaging subsystem that is analogous to conventional gantry mounted systems to create volumetric three-dimensional (3D) CBCT images of patients during or immediately before treatment. However, for our system, 3D image acquisition occurred under patient rotation so that anatomical deformation was coupled to rotation. This means that conventional tomography reconstruction techniques are suboptimal because using full 360-degree projections could introduce significant deformation artefact, or blur.

To minimize deformation blur, projections were sorted into angular bins, which cover a small range of patient rotation (Fig 2). Each angular bin was then reconstructed into a 3D image using an iterative digital-tomosynthesis reconstruction method. First, the reconstruction method required that the entire 360-degree projection set was used to reconstruct a deformation-blurred volume (f_{Blurred}) using the FDK algorithm. Then, the projection set was split into N_{Bin} angular-correlated bins with equal angular range. For this study, $N_{\text{Bin}} = 18$ with bins centered at 0, 20, …, 340 degrees was found to be an appropriate choice (ie, first bin: −10 to 10 degrees; second bin: 10-30

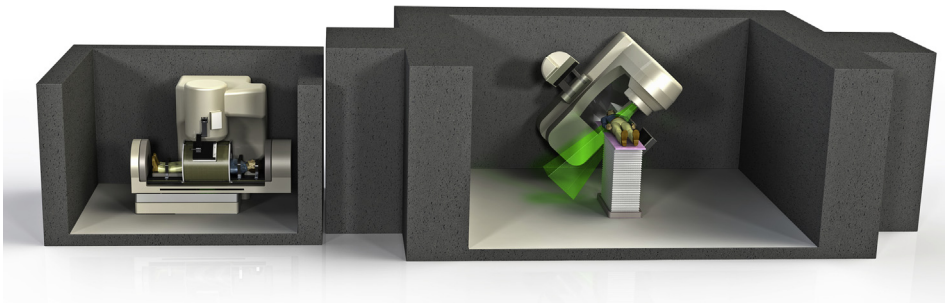

Figure 1 Comparison between our static gantry linac solution (left) and a conventional linac (right).

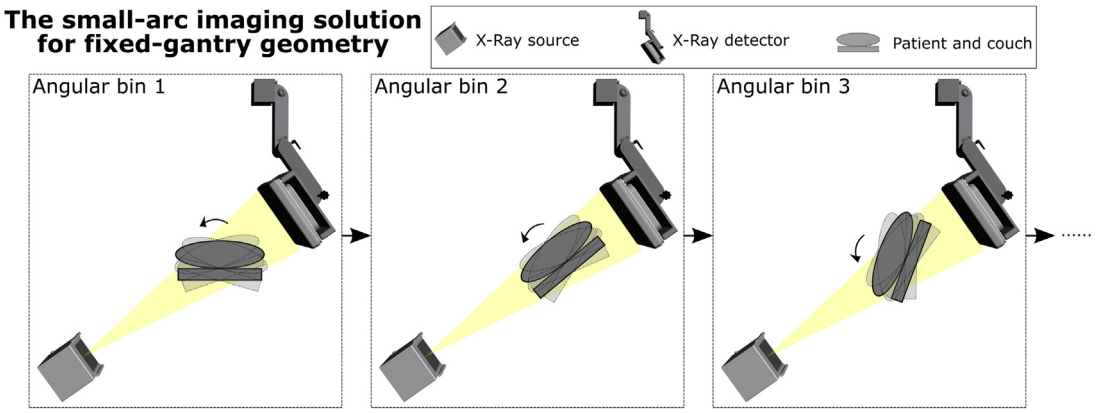

Figure 2 Our small arc imaging solution in which projections are sorted into angular bins and reconstructed into separate digital-tomosynthesis images.

degrees; etc.). Each angular bin was reconstructed in a separate volume using the prior image constrained compressed sensing (PICCS) algorithm[26] and f_{Blurred} as the common prior. The PICCS algorithm accounts for undersampled projection sets by adding a regularization term that combines a prior image similarty constraint and a total-variation constraint. This allows a 3D volume to be reconstructed with just a narrow angular range of projections. The output of this method is reconstructed 3D volumes with minimal deformation blur at various couch angles.

Results

Imaging equivalence

The volumetric images of the Catphan phantom reconstruction with fluoroscopic projections while the phantom rotated (Fig 3A) are equivalent (within 8% of the image intensity range) to the volumetric images that were reconstructed with projections acquired in a conventional manner with the gantry rotating. The difference image shows that the 2 images are almost identical except for small differences that can be observed around the edge of the phantom. The small differences were most likely caused by a misalignment between the couch rotation axis and the LINAC rotation axis, which is a limitation of this study. The line profile (Fig 3B) shows that the 2 images have a high agreement in both pixel intensities and spatial information. A histogram of the difference image is shown in Figure 3C. The mean absolute pixel value of the difference image was 28 Hounsfield units (HU) with a maximum value of 110 HU, which is comparable to uncertainties that are caused by Poisson noise. The spatial uncertainty, quantified by the maximum magnitude of the deformation vector field (DVF) between the 2 images obtained using B-spline transformation-based deformable image registration, was <1 mm.

Imaging under gravitational deformation

Figure 4 shows the conventional CBCT (porcine heart fixed at 0 degrees) and fixed-beam images (20-degree span in porcine heart rotation in each angular bin) of the porcine heart when viewed from different angles. The deformation between the conventional CBCT and fixed beam (static gantry) cases was quantified by the magnitude of the DVF between the 2 images, calculated via B-spline transformation-based deformable image registration. The 0-degree fixed-gantry, rotating phantom geometry reconstruction was found to coincide with the conventional CBCT image as shown in Figure 4A, with a mean magnitude of <3 mm and maximum magnitude of <5 mm of the DVF. This indicates an acceptable accuracy of the proposed reconstruction method for the static gantry acquisition. Similar accuracies can be inferred for the other angular bins despite the absence of ground truth comparisons because the reconstruction algorithm does not bias toward the 0-degree orientation. Gravitational deformation is expected to be the main contributing factor for the differences between the rotating phantom and conventional CBCT images for other angular bins, as shown in Figure 4B. The mean deformation magnitude ranged from 3.0 mm to 8.9 mm, with up to 16.1 mm maximum deformation. Deformation was mainly observed in the downward direction due to gravity, which is advantageous to the static gantry, horizontal patient rotation treatment geometry because the MV beam is aligned along the same direction.

Discussion

The inclusion of image guidance and adaptation enables a change in the patient setup paradigm, from the current iterative external or internal alignment to a patient-adaptive approach. Currently, patients are typically set up for treatment with 1 or a combination of

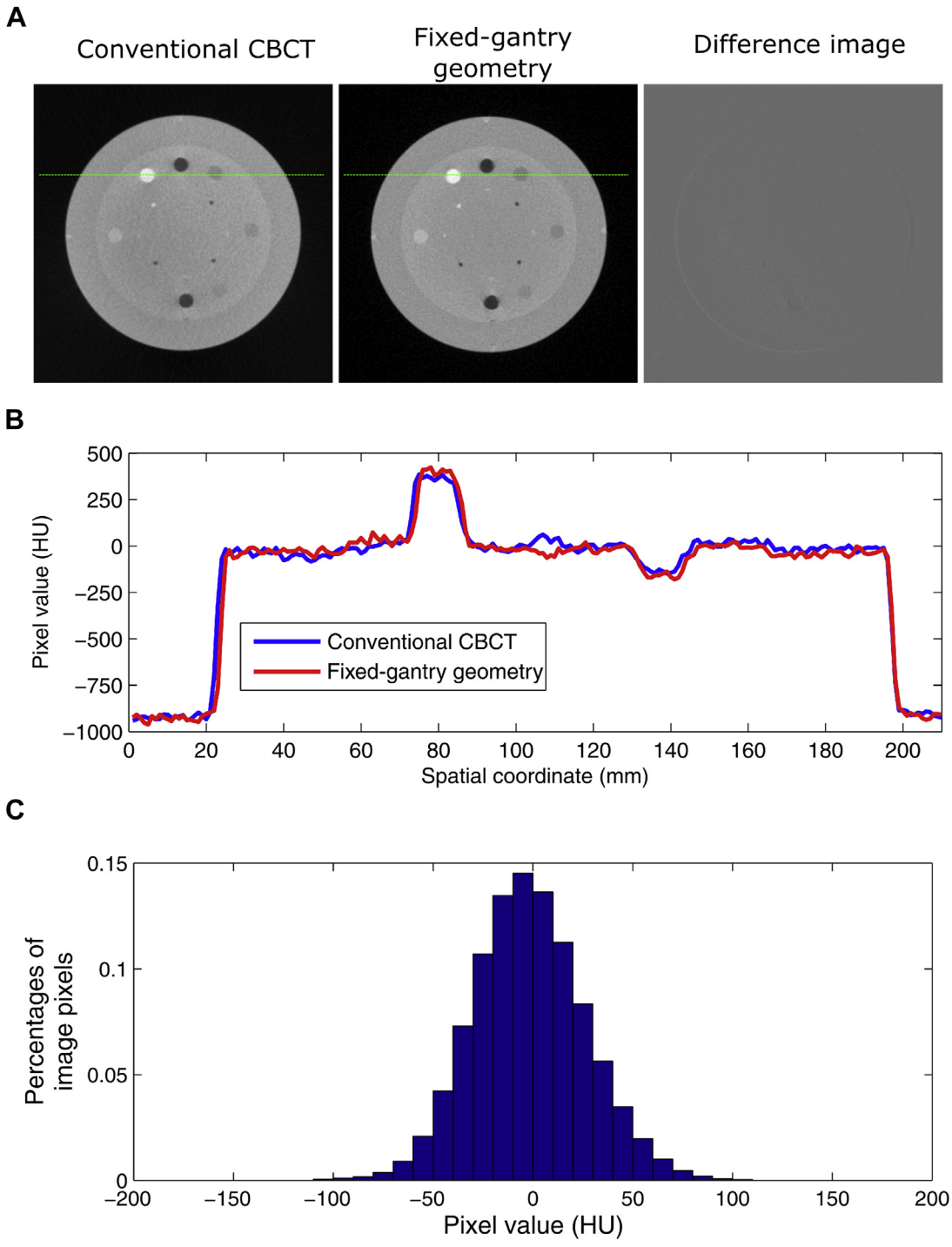

Figure 3 (A) Reconstructed Catphan images acquired with the conventional CBCT acquisition (left) and the static gantry acquisition (middle) (C/W = −250/1500 HU). The difference image is shown on the right (C/W = 0/1000 HU). (B) The intensity profiles extracted along the dashed line as shown in (A). (C) The histogram of the difference image. HU: Hounsfield unit.

room lasers, indexing systems, and x-ray imaging. The patient position is measured, corrected, and often measured again prior to treatment. In the patient-adaptive approach, variations in patient position and interfraction and intrafraction changes can be accounted for dosimetrically, even for large displacements. For example, for conformal prostate radiotherapy, shifts in patient positioning of up to 10 cm could be robustly adapted by geometry-based adaptation[27] and an intrafraction organ motion of 2 cm could be accounted for similarly.[28] For intensity modulated radiation therapy, geometry-based adaptation has been demonstrated to maintain plan quality despite target rotations of up to 5 degrees and translations up to 15 mm.[29] Having the system adapt

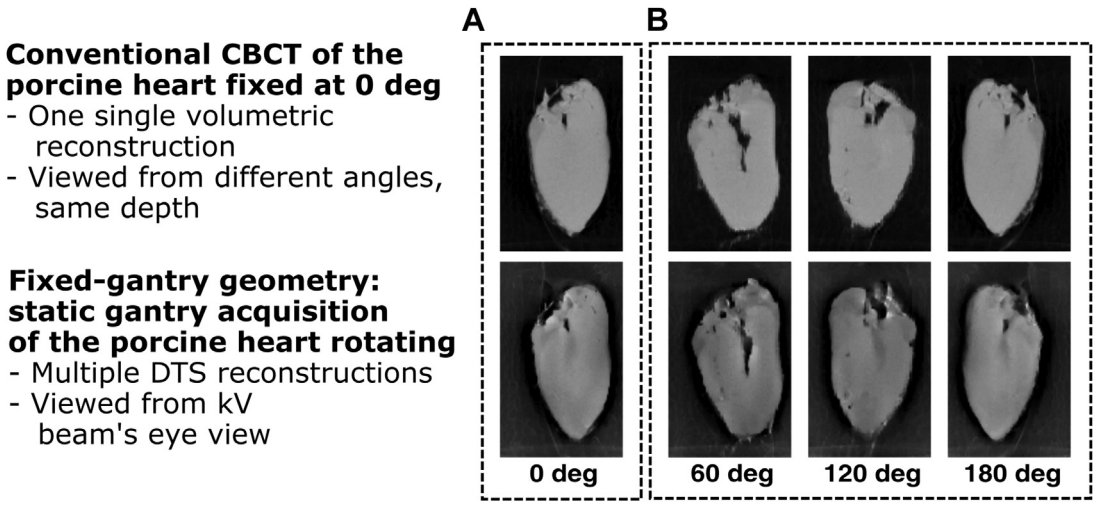

Figure 4 Images of the porcine heart acquired with conventional cone beam computed tomography (CBCT) (top) and our static gantry acquisitions (bottom). For the conventional CBCT case, different views of one single, reconstructed image with the porcine heart fixed at 0 degrees is shown. For the static gantry case, a separate reconstruction from each angular bin is shown. (A) The conventional CBCT image can be considered the ground truth for the 0-degree angular bin of the static gantry, rotating phantom reconstruction. (B) For all other angular bins, gravitational deformation is expected to be the main contributing factor for the differences between the conventional CBCT image and the rotating phantom images (C/W = −250/1500 HU).

to the patient rather than adapting the patient to the system will improve workflow when automation is sufficiently fast.

Comparison of proposed concept with existing treatment systems

Our concept is quite different from other treatment system machines that are currently available for megavoltage photonradiotherapy. The key differentiating features are patient rotation, which challenges image guidance, and immobilization, with reductions in the size, cost, and service burden of the rotating gantry. The gravitational effects on patient anatomy during rotation mean that real-time image guidance and adaptation could potentially be used to maintain treatment quality for curative patients. Overcoming this technological barrier means in a general sense that a large fraction of patients can be offered real-time imaging and adaptation. Marker-based real-time image guidance has been a clinical reality in real-time radiotherapy and CyberKnife[30] systems for more than a decade and recently has been implanted into a single-kV imager gantry rotating system,[31] which is an analog of our proposed single-kV imager patient rotating system. For widespread use, real-time image-guided radiation therapy will likely need markerless solutions. A variety of kV-based and MV-based solutions also have been proposed.[30,32-34] Much work is going into the broader clinical translation for these promising markerless methods.

Once the real-time image-guided radiation therapy system determines tumor location, the task of real-time adaptation to this motion can be achieved via multileaf collimator (MLC) tracking. MLC tracking technology has been clinically implemented for translational target tracking[35] and demonstrated to account for tumor rotation[36] and deformation[37] in phantom cases.

Accounting for gravitational deformation

One of the key challenges related to a static gantry (fixed-beam) treatment machine is accounting for gravitational deformation under patient rotation. The feasibility of correcting for gravitational deformation for CBCT was demonstrated with a porcine heart as a first step toward more realistic experiments. We are now investigating the effects of gravity on live animals and real patients. The effects of patent orientation, rotation speed, and the angular reproducibility of deformation will also be studied in extensive future work. A large library of patient magnetic resonance imaging (MRIs) under rotation will be acquired to support future studies with an MRI-compatible couch that has been built.

Gravitational deformation during treatment is addressed in terms of coarse and fine anatomic deformation. Adaptive plans built based on the CBCT at different patient rotation angles will be used to account for coarse anatomical deformation. Fine anatomic deformation will be adapted by MLC tracking.

Future work

The immediate next steps toward the development of our machine include validation of the functional dosimetric equivalence between our static gantry geometry

and a conventional rotating gantry treatment geometries; demonstration of a real-time imaging solution under our treatment geometry of true in vivo motion and deformation using small animals; magnetic resonance imaging of human organ motion and deformation using our MRI-compatible patient rotation couch; and development of a clinical prototype and demonstration-of-use cases for multiple cancer types, sites, and patient demographics.

Conclusion

In this paper, we have demonstrated the functional imaging equivalence between static gantry and conventional treatment and imaging geometries. We also demonstrated an initial method for real-time image reconstruction under horizontal patient rotation with a deformable phantom. This demonstration is a necessary first step toward solving the much larger clinical challenge of accounting for and adapting to patient motion and tissue deformation with a static gantry imaging system and a horizontally rotating patient.

Acknowledgments

The authors acknowledge the support of staff at the Nelune Comprehensive Care Centre at Prince of Wales Hospital and at Sydney University in Australia.

References

1. Bloom DE, Cafiero ET, Jane-Llopis E, et al. *The global economic burden of noncommunicable diseases*. Program on the Global Demography of Aging; 2012. Harvard School of Public Health, PGDA Working Paper No. 87. Available at: http://www.hsph.harvard.edu/pgda/working.htm. Accessed November 29, 2016.
2. Stewart BW, Wild S. Cancer worldwide. In: Stewart BW, Wild CP, eds. *World Cancer Report 2014*. Lyon, France: International Agency for Research on Cancer; 2014.
3. International Atomic Energy Agency. *Inequity in cancer care: A global perspective*. Vienna, Austria: IAEA Human Health Reports No. 3; 2011.
4. Barton MB, Jacob S, Shafiq J, et al. Estimating the demand for radiotherapy from the evidence: a review of changes from 2003 to 2012. *Radiother Oncol*. 2014;112:140-144.
5. IAEA. Directory of Radiotherapy Centres. Available at: https://nucleus.iaea.org/Pages/dirac.aspx. Accessed December 2015.
6. Atun R, Jaffray DA, Barton MB, et al. Expanding global access to radiotherapy. *Lancet Oncol*. 2015;16:1153-1186.
7. Zubizarreta EH, Fidarova E, Healy B, Rosenblatt E. Need for radiotherapy in low and middle income countries—the silent crisis continues. *Clin Oncol (R Coll Radiol)*. 2015;27:107-114.
8. Samiei M. Challenges of making radiotherapy accessible in developing countries. *Cancer Control*. 2013:85-96.
9. Heathcote KE, Armstrong BK. Disparities in cancer outcomes in regional and rural Australia. *Cancer Forum*. 2007;31:70-74.
10. Goldstein D, Margo J. Cancer in the bush. *Cancer Forum*. 2001;25.
11. Markossian TW, Hines RB, Bayakly R. Geographic and racial disparities in breast cancer—related outcomes in Georgia. *Health Serv Res*. 2014;49:481-501.
12. Radiation Oncology Tripartite Committee. *Planning for the Best: Tripartite National Strategic Plan for Radiation Oncology 2012–2022*. Sydney, Australia: The Royal Australian and New Zealand College of Radiologists. 2012.
13. World Health Organisation. *Global Action Plan for the Prevention and Control of Non-communicable Diseases*. Geneva, Switzerland: The World Health Organisation; 2013.
14. Chow AR, Boughey Z, Habermann EB. Rural women less likely to get radiation therapy after lumpectomy for breast cancer. *Forefront*. 2013;2.
15. Gabriel G, Barton M, Delaney GP. The effect of travel distance on radiotherapy utilization in NSW and ACT. *Radiother Oncol*. 2015;117:386-389.
16. Jong KE, Smith DP, Xue QY, et al. Remoteness of residence and survival from cancer in New South Wales. *Med J Aust*. 2004;180:618-622.
17. Baade PD, Dasgupta P, Aitken JF, et al. Distance to the closest radiotherapy facility and survival after a diagnosis of rectal cancer in Queensland. *Med J Aust*. 2011;195:350-354.
18. Le H, Penniment M, Carruthers S, Roos D, Sullivan T, Baxi S. Radiation treatment compliance in the Indigenous population: The pilot Northern Territory experience and future directions. *J Med Imaging Radiat Oncol*. 2013;57:218-221.
19. Valery PC, Coory M, Stirling J, Green AC. Cancer diagnosis, treatment, and survival in Indigenous and non-Indigenous Australians: A matched cohort study. *Lancet*. 2006;367:1842-1848.
20. Jaffray DA, Gospodarowicz M. Bringing global access to radiation therapy: Time for a change in approach. *Int J Radiat Oncol Biol Phys*. 2014;89:446-447.
21. Elekta. Compact. Available from: https://www.elekta.com/radiotherapy/treatment-delivery-systems/elekta-compact.html. Accessed November 29, 2016.
22. Department of Atomic Energy, Bhaba Atomic Research Centre. *Bhabhatron*. Available at: http://www.barc.gov.in/clip/bhabhatron.html. Accessed November 29, 2016.
23. Varian Medical Systems. *VitalBeam*. Available at: https://www.varian.com/en-gb/oncology/products/treatment-delivery/vitalbeam-radiotherapy-system. Accessed November 29, 2016.
24. Eslick EM, Keall PJ. The Nano-X Linear Accelerator a compact and economical cancer radiotherapy system incorporating patient rotation. *Technol Cancer Res Treat*. 2015;14:565-572.
25. Feldkamp LA, Davis LC, Kress JW. Practical cone-beam algorithm. *J Optical Soc Amer*. 1984;1:612-619.
26. Chen GH, Tang J, Leng S. Prior image constrained compressed sensing (PICCS): a method to accurately reconstruct dynamic CT images from highly undersampled projection data sets. *Med Phys*. 2008;35:660-663.
27. Lauve AD, Siebers JV, Crimaldi AJ, Hagan MP, Kealla PJ. A dynamic compensation strategy to correct patient-positioning errors in conformal prostate radiotherapy. *Med Phys*. 2006;33:1879-1887.
28. Keall PJ, Lauve AD, Hagan MP, Siebers JV. A strategy to correct for intrafraction target translation in conformal prostate radiotherapy: Simulation results. *Med Phys*. 2007;34:1944-1951.
29. Crijns W, Van Herck H, Defraene G, et al. Dosimetric adaptive IMRT driven by fiducial points. *Med Phys*. 2014;41:061716.
30. Ozhasoglu C, Saw CB, Chen H, et al. Synchrony—cyberknife respiratory compensation technology. *Medl Dosim*. 2008;33:117-123.
31. Keall PJ, Aun Ng J, O'Brien R, et al. The first clinical treatment with kilovoltage intrafraction monitoring (KIM): A real-time image guidance method. *Med Phys*. 2015;42:354-358.
32. Lin T, Cervino LI, Tang X, Vasconcelos N, Jiang SB. Fluoroscopic tumor tracking for image-guided lung cancer radiotherapy. *Phys Med Biol*. 2009;54:981-992.
33. Richter A, Wilbert J, Baier K, Flentje M, Guckeberger M. Feasibility study for markerless tracking of lung tumors in stereotactic body radiotherapy. *Int J Radiati Oncol Biol Phys*. 2010;78:618-627.

34. Rottmann J, Aristophanous M, Chen A, Court L, Berbeco R. A multi-region algorithm for markerless beam's-eye view lung tumor tracking. *Phys Med Biol*. 2010;55:5585-5598.
35. Colvill E, Booth JT, O'Brien RT, et al. MLC tracking improves dose delivery for prostate cancer radiotherapy: Results of the first clinical trial. *Int J Radiat Oncol Biol Phys*. 2015;92:1141-1147.
36. Wu J, Ruan D, Cho B, et al. Electromagnetic detection and real-time DMLC adaptation to target rotation during radiotherapy. *Int J Radiat Oncol Biol Phys*. 2012;82:e545-e553.
37. Ge Y, O'Brien RT, Shieh CC, Booth JT, Keall PJ. Toward the development of intrafraction tumor deformation tracking using a dynamic multi-leaf collimator. *Med Phys*. 2014;41:061703.